Contribution from Lehrstuhl für Anorganische Chemie I, Ruhr-Universität Bochum, D-4630 Bochum, FRG, and Anorganisch-Chemisches Institut der Universität Heidelberg, D-6900 Heidelberg, FRG

Novel Cofacial Bioctahedral Complexes of Ruthenium: Syntheses and Properties of the Mixed-Valence Species $[LRu^{2.5}(\mu\text{-}X)_3Ru^{2.5}L]^{2+}$ (X = Cl, Br, I, OH). Crystal Structures of $[LRu^{2.5}(\mu\text{-}OH)_3Ru^{2.5}L](PF_6)_2\cdot H_2O$ and $[LRu^{IV}(\mu\text{-}O)_3Ru^{IV}L](PF_6)_2\cdot H_2O$ (L = 1,4,7-Trimethyl-1,4,7-triazacyclononane)

Peter Neubold,[1a] Beatriz S. P. C. Della Vedova,[1a] Karl Wieghardt,*[,1a] Bernhard Nuber,[1b] and Johannes Weiss[1b]

Received December 14, 1989

Reaction of $RuCl_2(dmso)_4$ with 1,4,7-trimethyl-1,4,7-triazacyclononane (L; $C_9H_{21}N_3$) in ethanol affords red-brown $LRu(dmso)_xCl_2$ (x = 1-2), which reacted with concentrated HX (X = Cl, Br, I) in the presence of air to yield $LRuCl_3\cdot H_2O$, $LRuBr_3$, and $LRuI_3$. Treatment of these $LRuX_3$ species with CF_3SO_3H yielded gaseous HX and deep blue solutions from which the mixed-valence complexes $[L_2Ru_2^{2.5}(\mu\text{-}X)_3](CF_3SO_3)_2$ precipitated upon addition of ether. Blue $[L_2Ru_2^{2.5}(\mu\text{-}X)_3](PF_6)_2$ salts (X = Cl, Br, I) were isolated and characterized. Blue $[L_2Ru_2^{2.5}(\mu\text{-}OH)_3](PF_6)_2\cdot H_2O$ was synthesized from an aqueous solution of $[L_2Ru_2^{III}(\mu\text{-}O)(\mu\text{-}CH_3CO_2)_2](PF_6)_2$ via reduction with zinc amalgam and exposure of the resulting yellow solution to air. Oxidation of this species with $S_2O_8^{2-}$ at pH = 7 gave yellow $[L_2Ru_2^{III}(\mu\text{-}OH)_3](PF_6)_3$, which reacted at pH 12 with O_2 to yield green $[L_2Ru_2^{IV}(\mu\text{-}O)_3](PF_6)_2\cdot H_2O$. The crystal structures of $[L_2Ru_2^{2.5}(\mu\text{-}OH)_3](PF_6)_2\cdot H_2O$ (**1**) and $[L_2Ru_2^{IV}(\mu\text{-}O)_3](PF_6)_2\cdot H_2O$ (**2**) have been determined by X-ray analysis. Crystal data for **1**: orthorhombic space group *Pnma*, a = 10.089 (2) Å, b = 16.134 (3) Å, c = 19.585 (4) Å, V = 3188 (1) Å^3, Z = 4. Crystal data for **2**: orthorhombic space group *Pnma*, a = 10.057 (5), b = 16.12 (1) Å, c = 19.237 (9) Å, V = 3118.7 (10) Å^3, Z = 4. The $\{N_3Ru(O)_3RuN_3\}$ core in both structures possesses idealized D_{3h} symmetry. The Ru-Ru distances in **1** and **2** are 2.401 (2) and 2.363 (2) Å, respectively. Electronic and ESR spectra have been recorded, and the magnetic properties of complexes have been investigated. The electrochemistry of mononuclear and binuclear species are reported. The cyclic voltammogram of **2** in CH_3NO_2 displays two reversible one-electron waves at $E^1_{1/2}$ = -0.46 V and $E^2_{1/2}$ = +1.12 V vs NHE, which correspond to the couples

$$Ru^{III}Ru^{IV} \xrightleftharpoons{E^1_{1/2}} Ru_2^{IV} \xrightleftharpoons{E^2_{1/2}} Ru^{IV}Ru^{V}$$

Introduction

Mixed-valence binuclear $Ru^{II}Ru^{III}$ complexes of cofacial biooctahedral geometry that contain three μ-chloro or μ-bromo bridging ligands have received a great deal of attention during the past decades.[2] Symmetrical and unsymmetrical binuclear species have been synthesized and structurally characterized.[3,4] Their electronic structures have been investigated by various spectroscopic techniques with respect to delocalized or trapped valencies of the two ruthenium centers. Electrochemically, these $\{RuX_3Ru\}^{2+}$ complexes are often reversibly oxidized to yield the $\{Ru^{III}(\mu\text{-}X)_3Ru^{III}\}^{3+}$ core or reduced to produce the $\{Ru^{II}(\mu\text{-}X)_3Ru^{II}\}^{+}$ moiety.[3] Furthermore, Heath et al.[4] have shown that preparative-scale electrogeneration of $[Br_3Ru^{III}(\mu\text{-}Br)_3Ru^{IV}Br_3]^{2-}$ and even $[Ru_2^{IV}(\mu\text{-}Br)_3Br_6]^{-}$ is possible. Thus the binuclear cofacial octahedral complexes of D_{3h} symnmetry are available in a wide range of formal oxidation states.

An intriguing and very interesting question of fundamental importance is the degree of direct metal-metal interaction (metal-metal bond order) as a function of the formal oxidation state of the respective ruthenium centers in these triply bridged complexes. Obviously, an important parameter is the Ru-Ru distance in such species. However, since we are dealing with triply bridged binuclear species, this distance is interdependent with other structural parameters of the $\{M(\mu\text{-}X)_3M\}$ core, e.g. the M-X bond length and the M-X-M and the X-M-X bond angles. In other words, short M-M distances may be dictated by the steric requirements for the three bridging groups rather than direct metal-metal bonding. This point has been analyzed by Cotton and Ucko[5] and others.[6] To complicate matters further, in contrast to the well-documented series $Cr_2Cl_9^{3-}$, $Mo_2Cl_9^{3-}$, and $W_2Cl_9^{3-}$, where the former has no metal-metal bond and the latter two have a strong M-M bond, in the present binuclear ruthenium complexes the metal-metal bond is a priori weaker and the effect on the structure is less pronounced and not readily detectable.[8] On the basis of the very simple MO scheme for Ru_2 complexes (Scheme I) with D_{3h} symmetry[6,7] the formal metal-metal bond order (BO) increases on going from Ru_2^{II} (BO = 0), to $Ru_2^{2.5}$ (BO = 0.5), to Ru_2^{III} (BO = 1), to $Ru^{III}Ru^{IV}$ (BO = 1.5), and to Ru_2^{IV} (BO = 2) as electrons from antibonding orbitals a''_2 and e'' are stepwise removed. However, concomitant with the increasing Ru-Ru bond order, the Ru-X distances decrease due to the reduced effective ionic radii of the oxidized ruthenium centers, and again, one is faced with the problem of which factor is more important in determining the Ru-Ru distance: the increasing Ru-Ru bond order or the steric requirements of the contracted, face-sharing, triply bridged $\{Ru(\mu\text{-}X)_3Ru\}^{n+}$ core. Only the combination of

Scheme I

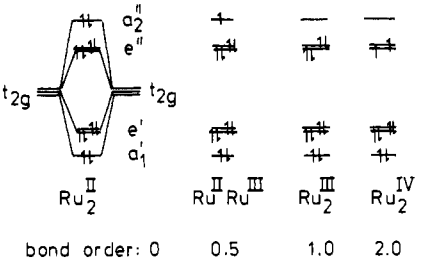

(1) (a) Ruhr-Universität Bochum. (b) Universität Heidelberg.
(2) (a) Schröder, M.; Stephenson, T. A. In *Comprehensive Coordination Chemistry*; Wilkinson, G., Gillard, R. D., McCleverty, J. A., Eds.; Pergamon Press: Oxford, England, 1987; Vol. 4, pp 277-478. (b) Seddon, K.; Seddon, E. A. The Chemistry of Ruthenium. In *Topics in Inorganic and General Chemistry*; Clark, R. J. H., Ed.; Elsevier: Oxford, England, 1984; Vol. 19.
(3) (a) Heath, G. A.; Lindsay, A. J.; Stephenson, T. A.; Vattis, D. K. *J. Organomet. Chem.* **1982**, *233*, 353. (b) Contreras, R.; Elliot, G. G.; Gould, R. O.; Heath, G. A.; Lindsay, A. J.; Stephenson, T. A. *J. Organomet. Chem.* **1981**, *215*, C6. (c) Heath, G. A.; Hefter, G.; Robertson, D. R.; Sime, W. J.; Stephenson, T. A. *J. Organomet. Chem.* **1978**, *152*, C1. (d) Easton, T.; Heath, G. A.; Stephenson, T. A.; Bochmann, M. *J. Chem. Soc., Chem. Commun.* **1985**, 154.
(4) Coombe, V. T.; Heath, G. A.; Stephenson, T. A.; Vattis, D. K. *J. Chem. Soc., Dalton Trans.* **1983**, 2307.
(5) Cotton, F. A.; Ucko, D. A. *Inorg. Chim. Acta* **1972**, *6*, 161.
(6) Summerville, R. H.; Hoffmann, R. *J. Am. Chem. Soc.* **1979**, *101*, 3821.
(7) Trogler, W. C. *Inorg. Chem.* **1980**, *19*, 697.
(8) See, for instance, the discussion of the bonding in $Ru^{III}_2Cl_6(PBu_3)_3$ where a Ru-Ru single bond is proposed (Ru-Ru = 3.176 (1) Å): Cotton, F. A.; Matusz, M.; Torralba, C. *Inorg. Chem.* **1989**, *28*, 1516.

0020-1669/90/1329-3355$02.50/0

structural data, magnetic properties, and electronic spectra of a *series* of similar complexes of the $\{Ru(\mu\text{-}X)_3Ru\}^{n+}$ type is likely to produce a definitive answer.

Species containing three chloro or bromo bridges have been fairly comprehensively characterized.[2] Ru–Cl and Ru–Br bonds are quite long (>2.2 Å), and therefore, we felt that the above question concerning direct metal–metal bonding in these species is complicated by the steric constraints imposed by these large halide bridges on the $\{Ru(\mu\text{-}X)_3Ru\}$ cores. Ru–OH or Ru–O bonds are significantly shorter and complexes containing three such bridges may be more informative. To our surprise, we found only very few examples of such species in the literature. It appears that only complexes with a $\{Ru^{II}(\mu\text{-}OH)_3Ru^{II}\}^{+}$ core have been structurally characterized.[9-11] No molecular species of the $\{Ru^{2.5}(\mu\text{-}OH)_3Ru^{2.5}\}^{2+}$ or $\{Ru_2^{III}(\mu\text{-}OH)_3\}^{3+}$ type have been described previously.

We report here the synthesis, magnetic, and spectroscopic properties of $[L_2Ru_2(\mu\text{-}OH)_3]^{2+/3+}$ and $[L_2Ru_2^{IV}(\mu\text{-}O)_3]^{2+}$ complexes all of which have been characterized by X-ray crystallography (L = 1,4,7-trimethyl-1,4,7-triazacyclononane). Their electrochemistry is also reported. Some aspects of this work have been communicated previously.[12] In addition, the mixed-valence complexes $[L_2Ru_2^{2.5}(\mu\text{-}X)_3]^{2+}$ (X = Cl, Br, I) have been synthesized from mononuclear precursors $LRuX_3$.

Experimental Section

The ligand 1,4,7-trimethyl-1,4,7-triazacyclononane (L)[13] and the complex $RuCl_2(dmso)_4$[14] were prepared according to published procedures.

$LRuX_3$ (X = Cl, Br, I). To a mixture of $RuCl_2(dmso)_4$ (1.0 g, 2.1 mmol) in absolute ethanol (25 mL) was added 1,4,7-trimethyl-1,4,7-triazacyclononane (0.80 g, 4.7 mmol) with stirring. The suspension was heated to 60 °C for 1 h until a clear deep red-brown solution was obtained, which was then heated under reflux for 2 h. The solvent was removed under reduced pressure by rotary evaporation. The red-orange residue ($LRu(dmso)_xCl_2$) was treated with concentrated HCl and heated under reflux for 30 min in the presence of air. An orange microcrystalline solid of $LRuCl_3\cdot H_2O$ precipitated, which was collected by filtration, washed with H_2O, ethanol, and diethyl ether, and air-dried. Upon reduction of the volume of the reaction mixture further product may be obtained (yield: 0.49 g, 60%).

Anal. Calcd for $C_9H_{23}N_3OCl_3Ru$: C, 27.2; H, 5.8; N, 10.5. Found: C, 27.6; H. 5.8; N, 10.5.

$LRuBr_3$ was prepared analogously by using concentrated HBr instead of HCl.

Anal. Calcd for $C_9H_{21}N_3Br_3Ru$: C, 21.1; H, 4.1; N, 8.2. Found: C, 20.9; H, 4.0; N, 8.1.

$LRuI_3$ was prepared analogously by using concentrated HI. The solution was heated to only 80 °C for 1 h.

Anal. Calcd for $C_9H_{21}N_3I_3Ru$: C, 16.5; H, 3.2; N, 6.4. Found: C, 16.7; H, 3.0; N, 6.3.

$[LRu(NCCH_3)_3](PF_6)_2$. To a solution of $LRuCl_3\cdot H_2O$ (0.15 g, 0.38 mmol) in acetonitrile (10 mL) was added zinc powder (0.15 g), and the mixture was heated to reflux for 20 min. The yellow solution was filtered, and a solution of $NaPF_6$ (0.4 g, 2.4 mmol) in CH_3CN (10 mL) was added. A yellow precipitate formed, which was filtered off and recrystallized from CH_3CN (yield: 0.10 g, 38%).

Anal. Calcd for $C_{15}H_{30}N_6P_2F_{12}Ru$: C, 26.3; H, 4.4; N, 12.3. Found: C, 26.0; H, 4.4; N, 12.1.

$[LRu^{2.5}(\mu\text{-}X)_3Ru^{2.5}L](PF_6)_2$ (X = Cl, Br, I). To solid $LRuX_3$ (0.6 mmol), where X represents Cl^-, Br^-, or I^-, was added trifluormethanesulfonic acid (20 mmol, 3.0 g) with cooling. Gaseous HX was pumped off. The reaction mixture was slowly allowed to warm up to room temperature with stirring. After 1 h, the reaction mixture was again cooled to 0 °C, and dry diethylether was carefully added with efficient cooling. The product $[LRu(\mu\text{-}X)_3RuL](CF_2SO_3)_2$ precipitated. After rapid filtration, the crude material was dissolved in water (5 mL). Solid $NaPF_6$ (0.75 g; 4.4 mmol) was added to this solution, which initiated the precipitation of the desired $[L_2Ru_2(\mu\text{-}X)_3](PF_6)_2$ salts, which were collected by filtration, washed with cold water, and dried over P_2O_5 in vacuo (yield: ≈45%).

Anal. Calcd for $C_{18}H_{42}Cl_3F_{12}N_6P_2Ru_2$: C, 23.0; H, 4.4; N, 8.9; Cl, 11.3. Found: C, 22.6; H, 4.4; N, 8.5; Cl, 11.3.

Anal. Calcd for $C_{18}H_{42}Br_3F_{12}N_6P_2Ru_2$: C, 20.1; H, 3.9; N, 7.8. Found: C, 19.9; H, 3.7; N, 7.7.

Anal. Calcd for $C_{18}H_{42}F_{12}N_6I_3P_2Ru_2$: C, 17.8; H, 3.5; N, 6.9. Found: C, 18.2; H, 3.5; N, 7.0.

$[LRu^{2.5}(\mu\text{-}OH)_3Ru^{2.5}L](PF_6)_2\cdot H_2O$. A 0.05 M H_2SO_4 solution was added to a mixture of $[L_2Ru_2^{III}(\mu\text{-}O)(\mu\text{-}CH_3CO_2)_2](PF_6)_2\cdot 0.5H_2O$[15] in water (15 mL) and 25 g of zinc amalgam (3%) under an argon atmosphere until the pH of the solution was 2. The solution was stirred for 2 h at 40 °C. To this clear yellow solution were added NaOH (pH = 12) and $NaPF_6$ (0.30 g; 1.8 mmol). The solution was then stirred in the presence of air at 40 °C until the color changed from yellow to deep blue. Slowly the precipitation of a blue microcrystalline product started. The mixture was stirred for another hour under an argon atmosphere and stored at 0 °C for 6 h. The blue precipitate was collected by filtration, washed with a small amount of ice-cold H_2O and dried in vacuo over P_2O_5. Recrystallization from a minimum amount of aqueous NaOH at (pH 10) produced single crystals suitable for an X-ray structure analysis (yield: 0.08 g, 35%).

Anal. Calcd for $C_{18}H_{47}F_{12}N_6O_4P_2Ru_2$: C, 23.9; H, 5.2; N, 9.3. Found: C, 24.1; H, 5.1; N, 9.4.

$[L_2Ru_2^{III}(\mu\text{-}OH)_3](PF_6)_3$. To a solution of $[L_2Ru_2^{2.5}(\mu\text{-}OH)_3](PF_6)_2\cdot H_2O$ (0.10 g, 0.10 mmol) in water (15 mL) was added a solution of $Na_2S_2O_8$ (0.04 g, 0.16 mmol) in H_2O (3 mL) at 35 °C. The color changed from deep blue to yellow within a few minutes. After the solution was heated at 90 °C for 2–3 min followed by the addition of $NaPF_6$ (0.25 g, 1.5 mmol), the reaction mixture was allowed to stand at 0 °C for 12 h. Yellow crystals precipitated, which were collected by filtration, washed with ethanol and ether, and air-dried (yield: 0.11 g, 95%).

Anal. Calcd for $C_{18}H_{45}N_6O_3P_3F_{18}Ru_2$: C, 21.0; H, 4.2; N, 8.2. Found: C, 20.8; H, 4.3; N, 7.9.

$[L_2Ru_2^{IV}(\mu\text{-}O)_3](PF_6)_2\cdot H_2O$. $[L_2Ru_2^{III}(\mu\text{-}OH)_3](PF_6)_3$ (0.10 g, 0.1 mmol) was dissolved in water (10 mL), and solid NaOH (0.02 g) was added with stirring. The solution was heated to 80 °C for 10 min during which time the color changed from yellow to deep green. $NaPF_6$ (0.05 g, 0.3 mmol) dissolved in H_2O (1 mL) was added to the hot solution. Dark green crystals precipitated within 12 h in the refrigerator at 0 °C. These were collected by filtration, washed with ethanol and ether, and air-dried (yield: 0.05 g, 60%).

Anal. Calcd for $C_{18}H_{44}N_6O_4P_2F_{12}Ru_2$: C, 23.5; H, 5.2; N, 9.0. Found: C, 23.8; H, 5.0; N, 9.1.

X-ray Crystallography. Intensities and lattice parameters of a needle-shaped, black crystal of $[L_2Ru_2(\mu\text{-}OH)_3](PF_6)_2\cdot H_2O$ (**1**) and a deep green, needle-shaped crystal of $[L_2Ru_2(\mu\text{-}O)_3](PF_6)_2\cdot H_2O$ (**2**) were measured on an AED II (Siemens) and a Syntex R3 diffractometer, respectively, at ambient temperature. Crystal parameters and details of the data collection and refinement are given in Table I (for full details

Table I. Crystallographic Parameters for $[L_2Ru_2(\mu\text{-}OH)_3](PF_6)_2\cdot H_2O$ (**1**) and $[L_2Ru_2(\mu\text{-}O)_3](PF_6)_2\cdot H_2O$ (**2**)

	1	**2**
fw	900.7	897.7
space group	*Pnma* (No. 62)	*Pnma* (No. 62)
a, Å	10.089 (2)	10.057 (5)
b, Å	16.134 (3)	16.12 (1)
c, Å	19.585 (4)	19.237 (9)
V, Å^3	3188 (1)	3118.7 (10)
Z	4	4
λ, Å	0.71073 (Mo Kα; graphite)	
ρ_{calcd}, g cm^{-3}	1.88	1.91
μ, cm^{-1}	11.32	11.57
T, °C	22	22
R	0.067	0.054
R_w	0.056	0.049

(9) (a) Arthur, T.; Robertson, D. R.; Tocher, D. A.; Stephenson, T. A. *J. Organomet. Chem.* **1981**, *208*, 389. (b) Gould, R. O.; Jones, C. L.; Stephenson, T. A.; Tocher, D. A. *J. Organomet. Chem.* **1984**, *264*, 365. (c) Robertson, D. R.; Stephenson, T. A. *J. Organomet. Chem.* **1976**, *116*, C29.

(10) Kim, T. D.; McNeese, T. J.; Rheingold, A. L. *Inorg. Chem.* **1988**, *27*, 2554.

(11) Ashworth, T. V.; Nolte, M. J.; Singleton, E. *J. Chem. Soc., Chem. Commun.* **1977**, 936.

(12) Neubold, P.; Della Vedova, B. S. P. C.; Wieghardt, K.; Nuber, B.; Weiss, J. *Angew. Chem.* **1989**, *101*, 780; *Angew. Chem., Int. Ed. Engl.* **1989**, *28*, 763.

(13) Wieghardt, K.; Chaudhuri, P.; Nuber, B.; Weiss, J. *Inorg. Chem.* **1982**, *21*, 3086.

(14) Evans, I. P.; Spencer, A.; Wilkinson, G. *J. Chem. Soc., Dalton Trans.* **1973**, 204.

(15) Neubold, P.; Wieghardt, K.; Nuber, B.; Weiss, J. *Inorg. Chem.* **1989**, *28*, 459.

Table II. Atom Coordinates ($\times 10^4$) and Temperature Factors ($Å^2 \times 10^3$) for $[L_2Ru_2(\mu\text{-}OH)_3](PF_6)_2 \cdot H_2O$

atom	x	y	z	U^a
Ru1	569 (1)	2500	370 (1)	28 (1)
Ru2	9280 (1)	2500	9340 (1)	25 (1)
O1	1200 (9)	2500	−575 (5)	30 (4)
O2	−701 (8)	1657 (4)	53 (3)	43 (3)
N1	−100 (18)	2500	1448 (8)	71 (8)
N2	2034 (10)	3396 (7)	747 (5)	50 (4)
C1	−1551 (19)	2500	1513 (10)	67 (10)
C2	464 (20)	3298 (14)	1722 (9)	218 (15)
C3	1630 (18)	3686 (9)	1421 (8)	94 (8)
C4	3286 (12)	2914 (8)	839 (9)	118 (9)
C5	2193 (14)	4104 (8)	279 (6)	64 (6)
N3	−2858 (11)	2500	−787 (7)	48 (6)
N4	−817 (10)	1620 (5)	−1502 (4)	43 (4)
C6	−3519 (18)	2500	−121 (10)	90 (12)
C7	−3191 (13)	3252 (9)	−1202 (9)	93 (8)
C8	−2272 (13)	1347 (11)	−1544 (10)	132 (10)
C9	−427 (19)	2087 (6)	−2138 (5)	100 (7)
C10	121 (14)	931 (7)	−1401 (7)	63 (6)
P1	1097 (4)	4743 (2)	3499 (2)	52 (1)
F11	2433 (10)	4683 (7)	3849 (6)	149 (6)
F12	895 (13)	3819 (5)	3408 (6)	162 (6)
F13	1294 (13)	5698 (7)	3579 (9)	226 (9)
F14	1859 (15)	4711 (9)	2841 (5)	245 (10)
F15	−258 (10)	4849 (9)	3156 (7)	223 (8)
F16	434 (15)	4681 (11)	4160 (6)	304 (11)
Wa1[b]	1604 (17)	7500	3671 (9)	143 (10)

[a] Equivalent isotropic U defined as one-third of the trace of the orthogonalized U_{ij} tensor. [b] Position of the oxygen atom of the water molecule of crystallization.

Table III. Atom Coordinates ($\times 10^4$) and Temperature Factors ($Å^2 \times 10^3$) for $[L_2Ru_2(\mu\text{-}O)_3](PF_6)_2 \cdot H_2O$

atom	x	y	z	U^a
Ru1	715 (1)	2500	5669.9 (6)	29.6 (4)
Ru2	−572 (1)	2500	4631.7 (6)	32.8 (4)
O1	−1202 (9)	2500	5562 (4)	32 (4)
O2	664 (8)	3327 (4)	4944 (4)	49 (2)
N1	2840 (12)	2500	5790 (7)	43 (5)
N2	826 (10)	3366 (6)	6498 (5)	49 (4)
C1	−3230 (14)	2091 (8)	4174 (10)	123 (9)
C2	−2170 (14)	923 (8)	4708 (7)	72 (6)
C3	−1532 (18)	1323 (8)	3586 (7)	104 (8)
C4	3470 (18)	2500	5129 (10)	95 (11)
C5	−109 (13)	4064 (8)	6388 (6)	59 (5)
N3	70 (17)	2500	3570 (8)	69 (7)
N4	−1987 (10)	1624 (7)	4248 (5)	53 (4)
C6	427 (19)	2906 (7)	7109 (6)	104 (8)
C7	1526 (19)	2500	3528 (10)	74 (10)
C8	3152 (15)	1759 (10)	6178 (9)	102 (8)
C9	2180 (16)	3677 (11)	6526 (10)	125 (10)
C10	−462 (20)	1704 (15)	3295 (10)	209 (14)
P1	1095 (4)	5252 (2)	8499 (2)	57 (1)
F11	908 (12)	6175 (6)	8409 (6)	154 (6)
F12	1289 (13)	4307 (7)	8557 (8)	205 (8)
F13	2434 (10)	5313 (7)	8841 (6)	153 (6)
F14	401 (15)	5287 (11)	9148 (5)	277 (10)
F15	−249 (10)	5139 (9)	8164 (7)	225 (8)
F16	1796 (15)	5243 (10)	7838 (5)	243 (9)
Wa1[b]	1570 (18)	2500	8655 (10)	181 (12)

[a] Equivalent isotropic U defined as one-third of the trace of the orthogonalized U_{ij} tensor. [b] Position of the oxygen atom of the water molecule of crystallization.

see Table S1 in the Supplementary Material). Empirical absorption corrections (ψ scans of seven reflections with $9 < 2\theta < 51°$) were carried out in each case.[16] Both structures were solved by conventional Patterson and difference Fourier methods. The function minimized during full-matrix least-squares refinements was $\sum w(|F_o| - |F_c|)^2$ where $w = 1/\sigma^2(I)$. Neutral-atom scattering factors and anomalous dispersion corrections for non-hydrogen atoms were taken from ref 17. The positions of the hydrogen atoms of the methylene groups were placed at calculated positions with d(C–H) = 0.96 Å and group isotropic thermal parameters while the methyl groups were treated as rigid bodies, each with three rotational variables. All non-hydrogen atoms were refined with anisotropic thermal parameters. Final positional parameters for **1** and **2** are given in Tables II and III, respectively.

Instrumentation. Magnetic susceptibilities of powdered samples were measured in the temperature range 90–298 K by using the Faraday method. The susceptibility of $[L_2Ru_2(\mu\text{-}O)_3](PF_6)_2 \cdot H_2O$ was measured in the range 2.3–299 K on a Foner magnetometer. Diamagnetic corrections were applied with use of Pascal's constants. X-band ESR-spectra were recorded on solid samples or frozen dmso solutions (f = 9.4217 GHz, P = 20 μW, modulation amplitude = 1 mT) on a Bruker ER 200 ESR spectrometer. Infrared spectra were recorded on a Perkin-Elmer 1720X FTIR spectrometer (KBr or CsI disks). The UV–vis/near-IR spectra were recorded on a Perkin-Elmer Lambda 9 spectrophotometer. The 400-MHz ^{1}H NMR spectra were recorded on a Bruker AM 400 FT spectrometer.

Electrochemistry. The apparatus used for electrochemical measurements has been described previously.[18] Cyclic voltammograms (CV) were usually recorded in acetonitrile (0.1 M tetra-*n*-butylammonium hexafluorophosphate, $[TBA]PF_6$, as supporting electrolyte) under an argon atmosphere. At the beginning of each experiment a CV of the solution containing only the supporting electrolyte was recorded. To this solution were then added solid samples ($\approx 10^{-3}$ M). A nearly equimolar amount of ferrocene was added as an internal standard. The working electrode was a platinum-button, glassy-carbon, or gold electrode; the reference electrode was an Ag/AgCl (saturated LiCl in C_2H_5OH) electrode and a Pt-wire auxiliary electrode was used. The redox potentials were measured against the internal standard ferrocenium/ferrocene

Scheme II

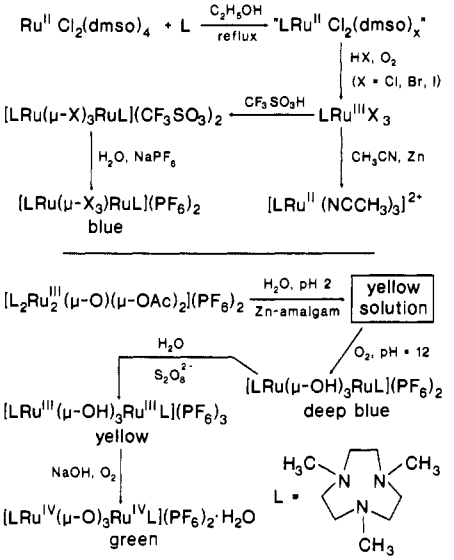

(Fc$^+$/Fc), for which a redox potential in CH_3CN of 0.40 V vs the normal hydrogen electrode (NHE) was assumed.[19] Criteria for the reversibility of electrode processes were those of Nicholson and Shain.[20]

Results and Discussion

Syntheses. Scheme II summarizes the synthetic routes and complexes prepared in this work. The reaction of $RuCl_2(dmso)_4$,[14] where dmso represents dimethyl sulfoxide, and the cyclic triamine L in refluxing ethanol affords a red-brown solution. Upon removal of the solvent under reduced pressure, a red-orange solid was obtained, the composition of which varied somewhat depending on the reaction conditions. Elemental analyses showed that the Ru:Cl ratio was constant at 1:2 but the ratio dmso:Cl varied between 2:2 and 3:2. The material is formulated as $[LRuCl_2$-

(16) Computations were carried out on an ECLIPSE computer by using the program package SHELXTL (Sheldrick, G. M. Universität Göttingen; Revision 5.1).
(17) *International Tables for X-ray Crystallography*; Kynoch: Birmingham, England, 1974; Vol. IV, pp 99, 149.
(18) Backes-Dahmann, G.; Herrmann, W.; Wieghardt, K.; Weiss, J. *Inorg. Chem.* **1985**, *24*, 485.
(19) (a) Koepp, H. M.; Wendt, H.; Strehlow, H. *Z. Elektrochem.* **1960**, *64*, 483; (b) Gagné, R. R.; Koval, C. A.; Lisensky, G. C. *Inorg. Chem.* **1980**, *19*, 2855.
(20) Nicholson, R. S.; Shain, I. *Anal. Chem.* **1965**, *37*, 178; **1964**, *36*, 706.

Table IV. Electronic Spectra and Magnetic Moments of Complexes

complex	λ_{max}, nm (ϵ = L mol^{-1} cm^{-1})[a]	magnetic moment, μ_B
$LRuCl_3 \cdot H_2O$	397 (2.3 × 10^3), 340 (sh), 300 (1.3 × 10^3)	2.35 (293 K), 1.94 (98 K)
$LRuBr_3$	not measured	2.11 (293 K), 1.96 (98 K)
$LRuI_3$	not measured	2.28 (293 K), 1.94 (103 K)
$[L_2Ru_2Cl_3](PF_6)_2$	1650 (300), 684 (6.15 × 10^3), 441 (805), 330 (970), 290 (sh)	1.88 (293 K), 1.90 (98 K)
$[L_2Ru_2Br_3](PF_6)_2$	763 (4.1 × 10^3), 474 (690), 340 (1.2 × 10^3), 300 (sh)	1.83 (293 K), 1.70 (98 K)
$[L_2Ru_2I_3](PF_6)_2$	742 (2.7 × 10^3)	2.20 (293 K), 1.99 (98 K)
$[L_2Ru_2(OH)_3](PF_6)_2 \cdot H_2O$	1540 (240), 648 (3.3 × 10^3), 354 (925)	1.75 (100–293 K)
$[L_2Ru_2(OH)_3](PF_6)_3$	1634 (320), 1450 (sh), 1150 (200), 1050 (200), 314 (7.4 × 10^3)	diamagnetic
$[L_2Ru_2(O)_3](PF_6)_2 \cdot H_2O$	1010 (900), 964 (750), 612 (460), 391 (1.9 × 10^3)	see text
$[LRu(NCCH_3)_3](PF_6)_2$	328 (265)	diamagnetic

[a] Measured in CH_3CN solution; extinction coefficients are per monomer or dimer.

$(dmso)_2](dmso)_x$ (x = 0–1). This solid proved to be a very useful starting material for compounds containing the LRu fragment. Thus heating mixtures of this complex and concentrated hydrohalic acids (HCl, HBr, HI) in the presence of air resulted in the formation of $LRuX_3$ species in good yields. Orange $LRuCl_3 \cdot H_2O$, red $LRuBr_3$, and brown $LRuI_3$ were obtained in this fashion in analytically pure form.

In an attempt to replace the halide ligands in the $LRuX_3$ species by a better leaving group such as the $CF_3SO_3^-$ ion, we treated these compounds with trifluormethanesulfonic acid with effective cooling of the reaction mixtures. In a very exothermic reaction, gaseous HX evolved, which was pumped off. The color of the solutions turned deep blue or black during this process. Addition of diethyl ether initiated the precipitation of deep blue microcrystalline solids of $[LRu^{2.5}(\mu\text{-}X_3)Ru^{2.5}L](CF_3SO_3)_2$. Thus dimerization with concomitant reduction to mixed-valence species and oxidation of X^- to X_2 is observed. We have not been able to synthesize a mononuclear $LRu^{III}(O_3SCF_3)_3$ complex via this route. Recrystallization of the above salts from water and addition of $NaPF_6$ yield the pure salts $[LRu^{2.5}(\mu\text{-}X)_3Ru^{2.5}L](PF_6)_2$ (X = Cl, Br, I).

Reduction of $LRuCl_3 \cdot H_2O$ in acetonitrile with zinc affords a yellow solution from which, upon addition of $NaPF_6$, yellow crystals of $[LRu^{II}(NCCH_3)_3](PF_6)_2$ precipitated.

Complexes containing three bridging hydroxo or oxo groups were prepared under anaerobic conditions from $[L_2Ru_2^{III}(\mu\text{-}O)(\mu\text{-}CH_3CO_2)_2](PF_6)_2$[15] by reduction of an acidic aqueous solution (pH = 2) of this species with zinc amalgam. The color of the violet solution changed to yellow. After removal of the Zn amalgam, the pH was adjusted to 12 (NaOH) in the presence of air and solid $NaPF_6$ was added. The color of the solution changed to deep blue, and crystals of $[L_2Ru_2^{2.5}(\mu\text{-}OH)_3](PF_6)_2 \cdot H_2O$ precipitated. Oxidation of an aqueous solution (pH = 7) of this complex with peroxodisulfate affords yellow crystals of the oxidized form $[L_2Ru_2^{III}(\mu\text{-}OH)_3](PF_6)_3$. Aqueous solutions of this species at pH > 12 were found to be air-sensitive. Thus the yellow color changed at 80 °C within 10 min to green. Addition of $NaPF_6$ initiated the precipitation of $[L_2Ru_2^{IV}(\mu\text{-}O)_3](PF_6)_2 \cdot H_2O$.

Spectroscopic and Magnetic Properties. (a) Monomers. In monomeric complexes $LRuX_3$, the N_3RuX_3 polyhedron possesses idealized C_{3v} symmetry since the cyclic triamine enforces a facial arrangement of the nitrogen and halogeno donor atoms, respectively. In the infrared spectrum of $LRuCl_3 \cdot 3H_2O$ (CsI disk), two Ru–N and two Ru–Cl stretching frequencies have been observed at 475, 440 cm^{-1} and 321, 297 cm^{-1}, respectively. Two bands at 258 and 230 cm^{-1} may be assigned to N–Ru–N deformation modes. The Ru–Cl frequencies are in good agreement with those reported for *fac*-$[Ru(NH_3)_3Cl_3]$[21] at 310 and 280 cm^{-1}.

The electronic spectrum of $LRuCl_3 \cdot H_2O$ displays three ligand-to-metal charge-transfer (CT) bands (Table IV). According to the established assignment of similar absorption maxima in $[RuCl_6]^{3-}$[22] the maxima at 397, 340, and 300 nm are $\pi \rightarrow t_{2g}$ CT bands. The low solubilities of $LRuBr_3$ and $LRuI_3$ in CH_3CN did not allow the recording of their solution spectra.

The magnetic moments of powdered samples of $LRuX_3$ complexes in the temperature range 98–298 K (Table IV) are typical for low-spin octahedral ruthenium(III) complexes. Due to large spin–orbit coupling at room temperature, these observed μ_{eff} values are larger than the spin-only value of 1.73 μ_B. The observed temperature dependence is in line with that for compounds such as $[Ru(NH_3)_6]^{3+}$[23] and $[Ru(NH_3)_5Cl]^{2+}$[23] and other octahedral Ru^{III} complexes.[2] The ESR spectrum of a solid sample of $LRuCl_3 \cdot H_2O$ at 10 K displays an axial g-value pattern. The spin Hamilonian for an isolated low-spin d^5 ruthenium(III) center (S = $^1/_2$) takes the form shown in eq 1.[24] Two resonances at $g_\parallel$ =

$$H = g_\parallel \beta H_z S_z + g_\perp \beta (H_x S_x + H_y S_y) \quad (1)$$

1.29 and $g_\perp$ = 2.92 are observed where the latter is more intense than the former.[25]

$[LRu^{II}(NCCH_3)_3](PF_6)_2$ is diamagnetic. Its electronic spectrum shows a maximum at 328 nm with a relatively large molar absorption coefficient of 265 L mol^{-1} cm^{-1}. In the 400-MHz ^{1}H NMR spectrum of this species in CD_3CN, a complicated multiplet is observed at 2.90 ppm (midpoint) (12 H), which is typical for methylene protons of the coordinated cyclic triamine and a singlet (9 H) for the three methyl groups of the cyclic amine at 2.85 ppm. The signal of the methyl protons of the coordinated acetonitrile ligands appear at δ = 2.45. The integral of this signal does not correspond to the expected nine protons since slow exchange of CH_3CN ligands by deuterated solvent molecules occurs. This has also been observed in $[Ru(CH_3CN)_6]^{2+}$ where the methyl proton signal was observed at δ = 2.59.[26]

(b) Binuclear $[LRu^{2.5}(\mu\text{-}X)_3Ru^{2.5}L]^{2+}$ (X = Cl, Br, I) Complexes. The data for the electronic spectra and magnetic properties for the mixed-valence complexes $[L_2Ru_2^{2.5}(\mu\text{-}X)_3](PF_6)_2$ are summarized in Table IV. Electronic absorption spectra were recorded in acetonitrile at ambient temperature. Spectra of the tris(μ-chloro) and the tris(μ-bromo) complexes are dominated by an intense absorption in the visible region and a weak absorption in the near-infrared region (near-IR), which have been assigned to $\sigma \rightarrow \sigma^*$ ($a_1' \rightarrow a_2''$) and $\delta^* \rightarrow \sigma^*$ ($e'' \rightarrow a_2''$) excitations according to Hush, Beattie, and Ellis[27] (Scheme I). Dubicki et al.[28] have concluded from MCD spectra of such complexes that the visible absorption must also contain a number of other electronic states of which one major component is the $\delta \rightarrow \pi$ ($e' \rightarrow e'$) ($^2E''$) transition.

The electronic spectrum of $[L_2Ru_2^{2.5}(\mu\text{-}OH)_3](PF_6)_2 \cdot H_2O$ is fully in accord with the above spectra (Figure 1). An intense

(21) Durig, J. R.; Omura, Y.; Mercer, E. E. *J. Mol. Struct.* **1975**, *29*, 53.
(22) Jørgensen, C. K. *Mol. Phys.* **1959**, *2*, 309.
(23) Figgis, B. W.; Lewis, J.; Mabbs, F. E.; Webb, G. A. *J. Chem. Soc. A* **1966**, 422.
(24) (a) Stanko, J. A.; Peresie, H. J.; Bernheim, R. A.; Wang, R.; Wang, P. S. *Inorg. Chem.* **1973**, *12*, 634. (b) Bunker, C.; Drago, R. S.; Hendrickson, D. N.; Richmann, R. M.; Kessell, S. L. *J. Am. Chem. Soc.* **1978**, *100*, 3805.
(25) Hathaway, B. J.; Billing, D. E. *Coord. Chem. Rev.* **1970**, *5*, 143.
(26) Rapaport, I.; Helm, L.; Merbach, A.; Bernhard, P.; Ludi, A. *Inorg. Chem.* **1988**, *27*, 873.
(27) Hush, N. S.; Beattie, J. K.; Ellis, V. M. *Inorg. Chem.* **1984**, *23*, 3339.
(28) (a) Dubicki, L.; Ferguson, J. *Chem. Phys. Lett.* **1984**, *109*, 129. (b) Dubicki, L.; Ferguson, J.; Krausz, E. R. *J. Am. Chem. Soc.* **1985**, *107*, 179. (c) Dubicki, L.; Ferguson, J.; Lay, P. A.; Maeder, M.; Magnuson, R. H.; Taube, H. *J. Am. Chem. Soc.* **1985**, *107*, 2167. (d) Dubicki, L.; Krausz, E. *Inorg. Chem.* **1985**, *24*, 4461.

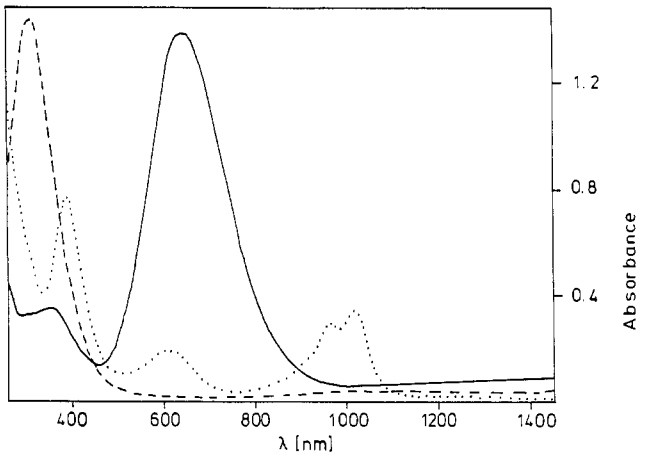

Figure 1. Electronic spectra of (a) $[L_2Ru_2(\mu\text{-}OH)_3](PF_6)_2\cdot H_2O$ (—), (b) $[L_2Ru_2(\mu\text{-}OH)_3](PF_6)_3$ (--), and (c) $[L_2Ru_2(\mu\text{-}O_3](PF_6)_2H_2O$ (···) in CH_3CN solutions and at 20 °C. Concentrations: (a) 3.8×10^{-4} M; (b) 1.95×10^{-4} M; (c) 3.7×10^{-4} M (1-cm cell). Absorption maxima in the near-IR region are listed in Table IV.

Table V. X-Band ESR Spectral Data for $[L_2Ru_2(\mu\text{-}X)_3](PF_6)_2$ Complexes at 10 K

	g values
$[L_2Ru_2Cl_3](PF_6)_2$	2.13, 1.90[a]
	2.12, 2.09, 1.90[b]
$[L_2Ru_2Br_3](PF_6)_2$	2.23, 2.03[b]
$[L_2Ru_2I_3](PF_6)_2$	2.23, 2.14, 1.95[a]
$[L_2Ru_2(OH)_3](PF_6)_2\cdot H_2O$	2.10, 2.02, 1.95[a]
	2.02, 1.94[b]

[a] Polycrystalline sample. [b] Frozen dmso solution.

absorption in the visible region at 648 nm ($\epsilon = 3.3 \times 10^3$ L mol^{-1} cm^{-1}) and an unsymmetrical low-intensity band at 1470 nm (ϵ = 240) are observed. The width at half-height, $\nu_{1/2}$, of both bands is significantly smaller than the $[2310\nu_{max}]^{1/2}$ [28] predicted for a class II complex according to the Robin and Day classification.[29] Furthermore, the peak position and width of the band in the near-IR region are independent of the polarity and nature of the solvent.[30] Spectra have been recorded in acetonitrile, dimethylformamide, acetone, water, nitromethane, ethanol, dichloromethane, dimethyl sulfoxide, and methanol: λ_{max} = 15 400 ± 150 cm^{-1}; $\nu_{1/2}$ = 4300 ± 100 cm^{-1} ($[2310\nu_{max}]^{1/2}$ = 6000 cm^{-1}). This is taken as clear evidence that the valences in $[L_2Ru_2(\mu\text{-}X)_3]^{2+}$ species (X = Cl, Br, OH) are delocalized; these complexes display typical class III behavior. It is noted that in unsymmetrical complexes containing the $\{Ru_2(\mu\text{-}X)_3\}^+$ core the degree of metal–metal interaction has been shown to decrease as the molecular asymmetry increases.[3a]

Magnetic moments of powdered samples of $[L_2Ru_2^{2.5}(\mu\text{-}X)_3](PF_6)_2$ (X = Cl, Br, I, OH) in the temperature range 90–298 K (Table IV) are in the range 1.88–2.20 μ_B, which indicates the presence of one unpaired electron.[3a] X-band ESR spectra of solid samples and frozen dmso solutions at 10 K were recorded; the results are summarized in Table V. Figure 2 shows the ESR spectra of $[L_2Ru_2^{2.5}(\mu\text{-}OH)_3](PF_6)_2\cdot H_2O$ (a) as a solid sample and (b) as a frozen dmso solution at 10 K. The former displays a rhombic *g* value pattern, but the solution spectrum shows a signal of uniaxial symmetry in agreement with the D_{3h} symmetry of the $\{N_3Ru(OH)_3RuN_3\}^{2+}$ core. For $[L_2Ru_2^{2.5}(\mu\text{-}Cl_3)](PF_6)_2$ the reverse is observed: a rhombic signal in frozen dmso and an axial signal in the solid state. The frozen dmso solution ESR spectrum of $[L_2Ru_2^{2.5}(\mu\text{-}Br)_3](PF_6)_2$ displays an axial signal. Due to the lability of $[L_2Ru_2^{2.5}(\mu\text{-}I)_3](PF_6)_2$ in dmso solution, only a polycrystalline sample was measured at 10 K. A rhombic signal is observed. ESR spectra of $[(NH_3)_6Ru_2(\mu\text{-}Cl)_3]^{2+}$ and of $[(NH_3)_6Ru_2(\mu\text{-}Br)_3]^{2+}$ in frozen glycerol/dmso at 60 K show ESR

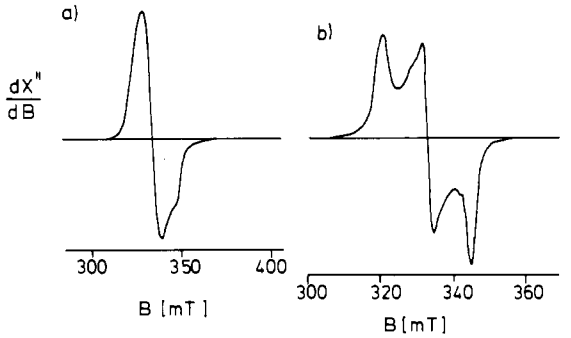

Figure 2. X-band ESR spectra of $[L_2Ru_2(\mu\text{-}OH)_3](PF_6)_2\cdot H_2O$ at 10 K: (a) frozen dmso solution; (b) solid sample.

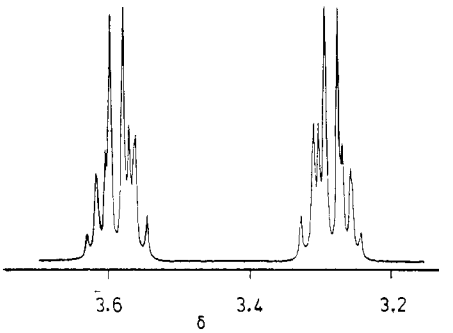

Figure 3. 400-MHz ^{1}H NMR spectrum of $[L_2Ru_2(OH)_3](PF_6)_3$ in CD_3CN. Signals of the methylene protons of the coordinated ligand are shown only.

spectra typical of a uniaxial species; the corresponding *g* values are very similar to those reported here. Other mixed-valence species exhibit similar *g*-value patterns.[3b] For a more detailed analysis of these ESR spectra, see ref 28d.

The yellow complex $[L_2Ru_2^{III}(\mu\text{-}OH)_3](PF_6)_3$ is diamagnetic in contrast to all tris(halogeno)-bridged complexes, which display residual paramagnetism. The only diamagnetic analogue is Wilkinson's organometallic complex $[(Me_3P)_6Ru_2^{III}(\mu\text{-}CH_2)_3]$, which contains a short Ru–Ru distance of 2.65 Å.[31] The 400-MHz ^{1}H NMR spectrum of the tris(μ-hydroxo) species in CH_3CN-d_3 displays four resonances: two complicated multiplets (Figure 3) centered at δ = 3.59 and 3.28 are assigned to the methylene protons of the coordinated triamines; a singlet of the six methyl groups at δ = 2.36 and a singlet of the OH protons at δ = 8.75 are observed. In the 100-MHz ^{13}C NMR spectrum (CH_3CN-d_3) a singlet at δ = 56.5 (CH_3 groups) and a singlet at δ = 64.6 (CH_2 groups) are observed. The NMR spectra are fully in accord with D_{3h} symmetry of the $\{N_6Ru_2(OH)_3\}^{3+}$ core in solution.

The electronic spectrum of $[L_2Ru_2^{III}(OH)_3]^{3+}$ exhibits an intense absorption maximum at 314 nm ($\epsilon = 7.4 \times 10^3$ L mol^{-1} cm^{-1}) which may be assigned to a $\sigma \rightarrow \sigma^*$ transition ($a_1' \rightarrow a_2''$) (Scheme I) and a series of weak transitions in the near-IR region (Table IV) of which one may be of the $\delta^* \rightarrow \sigma^*$ type. At present, we cannot assign these weak transitions in more detail but it is noted that octahedral monomeric $LRuX_3$ complexes do not show these absorption maxima. Interestingly and as is to be expected, the visible band ($\sigma \rightarrow \sigma^*$) is shifted to higher energy on going from the mixed-valence $\{Ru(OH)_3Ru\}^{2+}$ species to its oxidized form $\{Ru^{III}(OH)_3Ru^{III}\}^{3+}$.

The electronic spectrum of $[L_2Ru^{IV}_2(\mu\text{-}O)_3](PF_6)_2\cdot H_2O$ is also shown in Figure 1. We do not assign these bands because for reasons developed below it is not clear if a Ru^{IV}–Ru^{IV} bond exists or not.

Figure 4 shows plots of the magnetic moment, μ, and the molar susceptibility, χ_M, of $[L_2Ru_2^{IV}(\mu\text{-}O)_3](PF_6)_2\cdot H_2O$ vs. temperature. The latter exhibits a sharp increase of χ_M at temperatures below

(29) Robin, M. B.; Day, P. *Adv. Inorg. Chem. Radiochem.* **1967**, *10*, 247.
(30) Creutz, C. *Prog. Inorg. Chem.* **1983**, *30*, 1.
(31) Hursthouse, M. B.; Jones, R. A.; Malik, K. M. A.; Wilkinson, G. *J. Am. Chem. Soc.* **1979**, *101*, 4128.

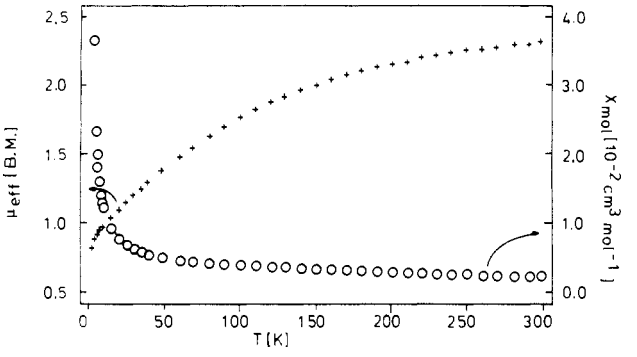

Figure 4. Plots of (a) molar susceptibility and (b) magnetic moment vs absolute temperature of $[L_2Ru_2(\mu\text{-}O)_3](PF_6)_2\cdot H_2O$.

Table VI. Selected Bond Distances (Å) and Angles (deg) for $[L_2Ru_2(\mu\text{-}OH)_3](PF_6)_2\cdot H_2O$ (**1**) and (in Parentheses) for $[L_2Ru_2(\mu\text{-}O)_3](PF_6)_2\cdot H_2O$ (**2**)

Ru1–O1	1.96 (1) (1.937 (9))	Ru1–O2	1.969 (7) (1.918 (7))
Ru1–N1	2.22 (2) (2.15 (1))	Ru1–N2	2.20 (1) (2.14 (1))
Ru2–O1	1.943 (9) (1.899 (6))	Ru2–O2	1.950 (7) (1.919 (7))
Ru2–N3	2.17 (1) (2.14 (1))	Ru2–N4	2.18 (1) (2.14 (1))
Ru1–Ru2	2.401 (2) (2.363 (2))		
O1–Ru1–O2	85.1 (3) (84.5 (3))	O1–Ru1–N1	178.8 (5) (178.9 (4))
O2–Ru1–N1	95.8 (4) (96.3 (3))	O1–Ru1–N2	95.7 (3) (97.2 (3))
O2′–Ru1–N2	177.4 (3) (176.5 (3))	N1–Ru1–N2	83.4 (4) (82.0 (4))
O2–Ru1–O2′	87.4 (4) (88.1 (4))	N2–Ru1–O2	95.1 (3) (95.1 (3))
N2–Ru1–N2′	82.4 (5) (81.6 (5))	O1–Ru2–O2′	85.9 (3) (85.5 (3))
O2′–Ru2–O2	88.4 (4) (88.0 (4))	O1–Ru2–N3	178.3 (5) (178.1 (5))
O2–Ru2–N3	95.2 (4) (95.9 (4))	O1–Ru2–N4	96.3 (4) (95.9 (3))
O2–Ru2–N4	176.0 (3) (177.1 (4))	O2′–Ru2–N4	95.0 (3) (94.6 (4))
N3–Ru2–N4	82.5 (4) (82.6 (4))	N4–Ru2–N4′	81.4 (5) (82.8 (6))
Ru1–O1–Ru2	76.0 (3) (76.1 (3))	Ru1–O2–Ru2	75.5 (3) (76.0 (3))

30 K, which indicates the presence of a paramagnetic impurity ($[L_2Ru_2(\mu\text{-}O)_3]^+$?). In the temperature range 50–300 K the magnetic moment varies between 1.39 and 2.31 μ_B per binuclear unit (or 0.98 and 1.63 μ_B per Ru^{IV} ion). At high temperatures, the magnetic moment per binuclear unit approaches the limit of $\approx$2.6 μ_B, which is close to the value of 2.83 μ_B expected for a triplet state ($S = 1$). This value would be in agreement with the simple molecular orbital scheme for a Ru–Ru bond of bond order 2 ($\sigma^2\pi^4\pi^{*2}$). On the other hand, a recent magnetochemical study by Hatfield, Meyer et al.[32] on the monomeric, octahedral oxoruthenium(IV) complex *cis*-$[Ru^{IV}(bpy)_2(py)(O)](ClO_4)_2$ has shown that this d^4 species has a nonmagnetic ground state with the first excited state lying 79 cm^{-1} higher in energy in the solid state. Thus the magnetic moment was found to vary between 1.95 μ_B at 50 K and $\approx$2.7 μ_B at 300 K per Ru^{IV} center. It is therefore conceivable that the observed temperature dependence of the present binuclear ruthenium(IV) complex is indicative of an antiferromagnetic exchange coupling between two independent face-sharing octahedral Ru(IV) centers. Attempts to model the magnetic behavior by using the simple Heisenberg, Dirac, and van Vleck spin-exchange model ($H = -2J\hat{S}_1\hat{S}_2$, $S_1 = S_2 = 1$) have failed. A more sophisticated treatment involving different models is obviously called for.

Interestingly, very similar magnetic properties have been reported for the high pressure phase of $BaRu^{IV}O_3$ and $Ba_{5/6}Sr_{1/6}Ru^{IV}O_3$ where binuclear face-sharing entities $\{O_3Ru_2O_3RuO_3\}$ are linked to chains via corner sharing.[33-35] For comparison, the magnetic moments per Ru^{IV} center in $Ba_{5/6}Sr_{1/6}Ru^{IV}O_3$ are 0.6 μ_B at 50 K and 1.25 μ_B at 300 K.[35]

Crystal Structures. $[L_2Ru_2^{2.5}(\mu\text{-}OH)_3](PF_6)_2\cdot H_2O$ (**1**) and $[L_2Ru_2^{IV}(\mu\text{-}O)_3](PF_6)_2\cdot H_2O$ (**2**) crystallize in the orthorhombic space group *Pnma*, and the respective lattice parameters are very similar. The unit cell volume of **1** is slightly larger than that of **2** in agreement with the fact that the Ru–N and Ru–O bond distances of the binuclear cation in **1** are slightly larger than those in **2**. Parts a and b of Figure 5 show the structures of the dications in **1** and **2**, respectively. Selected bond distances and angles are summarized in Table VI.

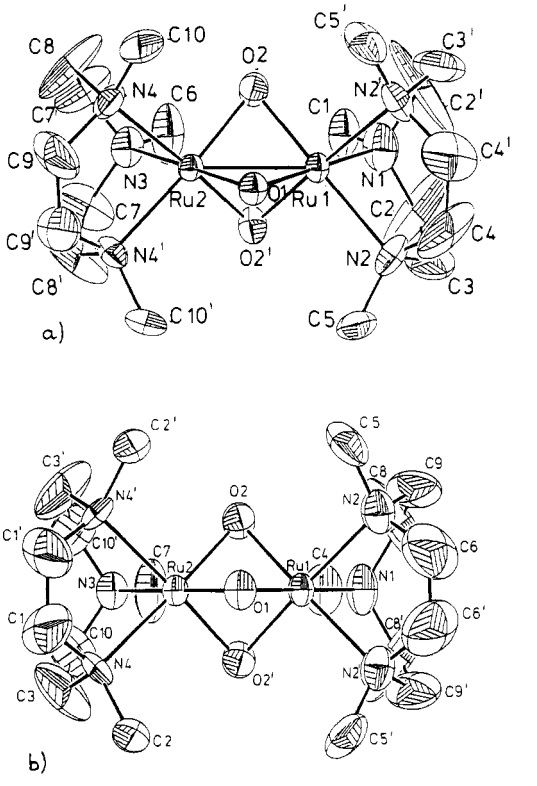

Figure 5. Structures and atom-labeling schemes for the dications in (a) $[L_2Ru_2(\mu\text{-}OH)_3](PF_6)_2\cdot H_2O$ and (b) $[L_2Ru_2(\mu\text{-}O)_3](PF_6)_2\cdot H_2O$.

The dications possess crystallographically imposed site symmetry *m*; atoms Ru1, Ru2, O1, N3 and N1 lie on this mirror plane, which bisects the binuclear cations in both structures. Since the site symmetry *m* is not compatible with the ($\lambda\lambda\lambda$) or ($\delta\delta\delta$) conformation of the five-membered Ru–N–C–C–N chelate rings of the capping tridentate amine ligands L, the thermal ellipsoids of the methylene carbon atoms are unrealistically large and physically meaningless. They reflect a disorder that we have not been able to model satisfactorily by a split-atom model. This behavior is frequently encountered in crystal structure determinations of complexes containing coordinated 1,4,7-triazacyclononane ligands.[36]

The structures of the dications in crystals of **1** and **2** consist in each case of two ruthenium ions bridged by either three μ-hydroxo or three μ-oxo ions. Pseudooctahedral coordination at each Ru is completed by a facially coordinated 1,4,7-trimethyl-1,4,7-triazacyclononane ligand. Thus the cations are cofacial bioctahedral. The most intriguing facet of these two structures are the short Ru–Ru distances of 2.401 (2) Å in **1** and 2.363 (2) Å in **2**. For comparison, pertinent distances and angles of a number of face-sharing bioctahedral complexes of Ru are summarized in Table VII.

It appears to be a common feature of cofacial binuclear ruthenium complexes that a considerable shortening of the Ru–Ru distance occurs upon one-electron oxidation of the $\{Ru^{II}(\mu\text{-}X)_3Ru^{II}\}^+$ core to $\{Ru_2(\mu\text{-}X)_3\}^{2+}$ species. This difference is about 0.6 Å for the tris(μ-chloro) *and* the tris(μ-hydroxo) species. This is indicative of a direct Ru–Ru bonding interaction in the mixed-valence forms. In D_{3h} symmetry the t_{2g} orbitals of octahedral ruthenium centers form a σ (a_1') and two π (e′) bonding molecular orbitals and a σ^* (a_2'') and two π^* (e″) orbitals (Scheme I).[5-7] In the case of Ru_2^{II}, 12 electrons occupy these six orbitals, and

(32) Dobson, J. C.; Helms, J. H.; Doppelt, P.; Sullivan, B. P.; Hatfield, W. E.; Meyer, T. J. *Inorg. Chem.* **1989**, *28*, 2200.
(33) Longo, J. M.; Kafalas, J. A. *Mater. Res. Bull.* **1968**, *2*, 687.
(34) Donohue, P. C.; Katz, L.; Ward, R. *Inorg. Chem.* **1966**, *5*, 335.
(35) Calaghan, A.; Moeller, C. W.; Ward, R. *Inorg. Chem.* **1966**, *5*, 1572.
(36) Chaudhuri, P.; Wieghardt, K. *Prog. Inorg. Chem.* **1987**, *35*, 329.

Table VII. Comparison of Structural Data for Face-Sharing Bioctahedral Complexes Containing a $M(\mu\text{-}X)_3M$ Core (X = OH, O, Cl, Br)

complex	M···M, Å	M–X, Å	M–X–M, deg	X–M–X, deg	ref
$[Ru^{II}_2(\mu\text{-}OH)_3(PMe_2Ph)_6][BPh_4]$	3.08	2.15–2.21	90	75	11
$[Ru^{II}_2(\mu\text{-}OH)_3(\eta^6\text{-}C_6H_6)_2]Cl\cdot 3H_2O$	2.9812 (7)	2.080 (3)	91.5		10
$[Ru^{II}_2(\mu\text{-}OH)_3(\eta^6\text{-}1,3,5\text{-}C_6H_3Me_3)_2]Cl\cdot 3H_2O$	2.989 (3)	2.09 (1)	90.9 (4)	75.3 (5)	9b
$[L_2Ru^{2.5}_2(\mu\text{-}OH)_3](PF_6)_2\cdot H_2O$	2.401 (2)	1.955 (10)	75.7	86.7	this work
$[L_2Ru^{III}_2(\mu\text{-}OH)_3](ClO_4)_3$	2.505 (3)	2.06	75.0	88.0	this work
$[Ru^{III}_2(\mu\text{-}CH_2)_3(Me_3P)_6]$	2.650 (1)	2.107	78.0	83	31
$[Ru^{II}_2(\mu\text{-}Cl)_3(MeC(CH_2PPh_2)_3)_2]BPh_4$	3.455 (1)	2.494 (3)	87.8	78.0	39
$[Ru^{II}_2(\mu\text{-}Cl)_3(PEt_2Ph)_6]^+$	3.444 (4)	2.48	87.7	76.9	40
$[Ru^{II}_2(\mu\text{-}Cl)_3(PMe_2Ph)_6]^+$	3.39	2.49	86	79	41
$[Ru^{2.5}_2(NH_3)_6(\mu\text{-}Cl)_3][BPh_4]_2$	2.753	2.393	70.2	90.3	37
$[Ru^{2.5}_2(NH_3)_6(\mu\text{-}Br)_3][ZnBr_4]$	2.852 (4)	2.53 (3)	68.5	92.4	38
$[Ru^{III}_2Cl_6(PBu_3)_3]$	3.176 (1)	2.456	80.7	85	8
$[Ru^{IV}_2L_2(\mu\text{-}O)_3](PF_6)_2\cdot H_2O$	2.363 (2)	1.918	76	86.5	this work
$[Mn^{IV}_2L_2(\mu\text{-}O)_3](PF_6)_2\cdot H_2O$	2.296 (2)	1.822	78.1	84.3	42
$[Cr^{III}_2L_2(\mu\text{-}OH)_3]I_3\cdot 3H_2O$	2.642 (2)	1.972			13
$[Co^{III}_2(NH_3)_6(\mu\text{-}OH)_3]^{3+}$	2.565	1.93 (1)	83.3 (6)	80.7 (3)	43

the resulting formal bond order is zero. Upon oxidation to $Ru_2^{2.5}$ dimers one antibonding electron is removed and the Ru–Ru bond order is formally 0.5 ($\sigma^2\pi^4\pi^{*3}$).

However, Cotton and Ucko[5] have pointed out that in bridged metal dimers some of the structural variables are interdependent, and appreciable metal–metal bonding in triply bridged cofacial complexes should enforce M–X–M angles smaller than 70.5° and X–M–X angles greater than 90°. The classic example is the series of $[M_2Cl_9]^{3-}$ complexes (M = Cr, Mo, W).[6] If these criteria are strictly applied for the present series (Table VII) only in the $[(NH_3)_6Ru_2^{2.5}(\mu\text{-}Cl)_3]^{2+}$ [37] complex and its tris(μ-bromo) analogue[38] is Ru–Ru bonding indicated, whereas in the tris(μ-hydroxo) complex (**1**) the short Ru–Ru distance could be a consequence of the geometric constraints imposed by three bridging hydroxo ligands. Interestingly, a short Fe···Fe distance of 2.509 (6) Å in the analogous mixed-valent $[L_2Fe^{2.5}_2(\mu\text{-}OH)_3](ClO_4)_2\cdot CH_3OH\cdot 2H_2O$ underscores this point[44] since the high-spin (hs) iron(II) and iron(III) ions are ferromagnetically coupled (μ = 9,5 μ_B per binuclear dication) and no Fe···Fe bond is formed. The same argument is true for $[(NH_3)_3Co^{III}(\mu\text{-}OH)_3Co^{III}(NH_3)_3]^{3+}$ where the Co···Co distance is 2.565 Å[43] and for $[L_2Cr^{III}_2(\mu\text{-}OH)_2]I_3\cdot 3H_2O$[13] where a Cr···Cr distance of 2.642 (2) Å has been observed. The latter three complexes do not have direct bonding metal–metal interactions. Therefore, although the Ru···Ru distance decreases by 0.6 Å upon oxidation from $\{Ru_2^{II}(\mu\text{-}OH)_3\}^+$ to $\{Ru_2^{2.5}(\mu\text{-}OH)_3\}^{2+}$, the structural features *alone* do not conclusively support the view that a Ru–Ru bond is formed. However the electronic and the magnetic properties of **1** in conjunction with the structural data support this view more rigorously.

The question as to whether a Ru–Ru bond is formed also arises for $[L_2Ru_2^{III}(\mu\text{-}OH)_3](ClO_4)_3\cdot H_2O$ and even more so for $[L_2Ru_2^{IV}(\mu\text{-}O)_3](PF_6)_2\cdot H_2O$. For the former, crystals of very low X-ray quality were obtained and the structure has been solved and refined to a conventional *R* factor of 0.086 in the trigonal space group $P31c$ (C_{3v}^4), with a = 9.897 (6) Å and c = 21.17 (1) Å. The standard deviations of bond distances and angles are large, but the structure determination clearly revealed the connectivity of atoms to be same for the trication as in the dication of **1**. A fairly reliable Ru–Ru distance of 2.505 (3) Å has been determined. This is the shortest Ru^{III}–Ru^{III} distance reported for a cofacial binuclear Ru_2^{III} complex. In Cotton's complex $[Ru_2^{III}Cl_6(PBu_3)_3]$, this distance is 3.176 (1) Å.[8] In Wilkinson's diamagnetic complex $[Ru_2^{III}(\mu\text{-}CH_2)_3(PMe_3)_6]$, a short Ru–Ru distance of 2.650 (1) Å has been interpreted as a Ru–Ru bond of order 1.[31] Consequently, we propose a metal bond ($\sigma^2\pi^4\pi^{*4}$) for $[L_2Ru_2^{III}(\mu\text{-}OH)_3]^{3+}$, which is supported by its diamagnetism. In contrast, $\{Ru^{III}(\mu\text{-}Cl)_3Ru^{III}\}^{3+}$ and their tris(μ-bromo) analogues show residual paramagnetism,[3b] but their structures have not as yet been determined by X-ray crystallography (Ru···Ru distances of >2.8 Å are expected). Finally, in diamagnetic $[([9]aneN_3)_2Ru_2^{III}(\mu\text{-}OH)_2(\mu\text{-}CH_3CO_2)]I_3\cdot H_2O$, a Ru–Ru single bond at 2.572 (3) Å has been observed ($\sigma^2\pi^2\delta^2\delta^{*2}\pi^{*2}$) that in this instance is clearly established by its structural features, i.e. acute Ru–OH–Ru and obtuse HO–Ru–OH bond angles.[45]

In $[L_2Ru_2^{IV}(\mu\text{-}O)_3](PF_6)_2\cdot H_2O$ an extremely short Ru–Ru distance of 2.363 (2) Å appears to be in agreement with a metal–metal bond formally of the bond order 2 ($\sigma^2\pi^4\pi^{*2}$). This may also be in accord with its magnetism. The effective magnetic moment approaches at temperatures >300 K the spin-only value for two unpaired electrons per binuclear unit (Scheme I).

However, the structural data alone do not provide conclusive evidence for metal–metal bonding as is readily seen from a comparison with other tris(μ-oxo)-bridged structures (Table VII). In $[L_2Mn_2^{IV}(\mu\text{-}O)_3]^{2+}$, a very short Mn···Mn distance of 2.296 (2) Å and a very strong antiferromagnetic coupling between the two d^3 centers ($H = -2J\hat{S}_1\cdot\hat{S}_2$; $S_1 = S_2 = {}^3/_2$; $J = -390$ cm^{-1}) has been observed.[42] The M–O–M angles in both structures are larger than 70.5° (76° for Ru_2^{IV} and 78.1 for Mn_2^{IV}) and the O–M–O angles are both smaller than 90°. These angles are again quite similar to those in complexes with an $\{M(\mu\text{-}OH)_3M\}^{3+}$ core (M = Co, Cr) where no metal–metal bonding occurs.[13,43] It should also be kept in mind that the d orbitals of a ruthenium(IV) ion are more contracted as compared to their reduced forms Ru^{III} and Ru^{II}.

The average Ru^{IV}–O_b bond length in **2** is 1.918 Å, which is longer than the corresponding distance in $K_4[Cl_5Ru\text{–}O\text{–}RuCl_5]$ containing a linear $\{Ru\text{–}O\text{–}Ru\}^{6+}$ unit.[46] In μ-hydroxy-bridged complexes of Ru^{III}, Ru–$O_{hydroxo}$ bond lengths of 2.02 Å have been observed; this distance is 1.97 Å in the mixed-valence complex **1**.

In summary, on the basis of the structural data for $[L_2Ru_2^{2.5}(\mu\text{-}OH)_3](PF_6)_2\cdot H_2O$, $[L_2Ru_2^{III}(\mu\text{-}OH)_3](ClO_4)_3$ and $[L_2Ru_2^{IV}(\mu\text{-}O)_3](PF_6)_2\cdot H_2O$ alone an unambiguous assignment of metal–metal bonding is not possible—despite two short and a very short Ru–Ru distance. In conjunction with their electronic spectra and magnetic properties, it appears to be reasonably safe to invoke such Ru···Ru interactions at least for the former two complexes. The structural and magnetic properties of

(37) Hughes, M. N.; O'Reardon, D.; Poole, R. K.; Hursthouse, M. B.; Thornton-Pett, M. *Polyhedron* **1987**, *6*, 1711.
(38) Beattie, J. K.; Favero, P.; Hambley, T. W.; Hush, N. S. *Inorg. Chem.* **1988**, *27*, 2000.
(39) Rhodes, L. F.; Sorato, C.; Venanzi, L. M.; Bachechi, F.; *Inorg. Chem.* **1988**, *27*, 604.
(40) Raspin, K. A. *J. Chem. Soc. A* **1969**, 461.
(41) Laing, M.; Pope, L. *Acta Crystallogr., Sect. B: Struct. Crystallogr. Cryst. Chem.* **1976**, *B32*, 1547.
(42) Wieghardt, K.; Bossek, U.; Nuber, B.; Weiss, J.; Bonvoisin, J.; Corbella, M.; Vitols, S. E.; Girerd, J. J. *J. Am. Chem. soc.* **1988**, *110*, 7398.
(43) Thewalt, U. *Z. Anorg. Allg. Chem.* **1975**, *412*, 29.
(44) Drüeke, S.; Chaudhuri, P.; Pohl, K.; Wieghardt, K.; Ding, X. Q.; Bill, E.; Sawaryn, A.; Trautwein, A. X.; Winkler, H.; Gurman, S. J. *J. Chem. Soc., Chem. Commun.* **1989**, 59.
(45) Wieghardt, K.; Hermann, W.; Köppen, M.; Jibril, I.; Huttner, G. *Z. Naturforsch.* **1984**, *39b*, 1335.
(46) Deloume, J. P.; Faure, R.; Thomas-David, G. *Acta Crystallogr., Sect. B: Struct. Crystallogr. Cryst. Chem.* **1979**, *B35*, 558.

Table VIII. Electrochemical Data for the Complexes[a]

complex	$E_{1/2}$, V	E_p, V
$LRuCl_3$[b]	+1.18[d]	−0.59[e]
$LRuBr_3$[b]	+1.14[d]	−0.46[e]
$[LRu(NCCH_3)_3](PF_6)_2$[b]	+1.31[d]	
$[L_2Ru_2Cl_3](PF_6)_2$[b]	+1.01, −0.19[d]	
$[L_2Ru_2Br_3](PF_6)_2$[c]	+0.93, −0.09[d]	
$[L_2Ru_2I_3](PF_6)_2$[c]	+0.90, +0.05[d]	
$[L_2Ru_2(OH)_3](PF_6)_2 \cdot H_2O$[b]	−0.11[d]	−1.30[e]
$[L_2Ru_2(\mu\text{-}O)_3](PF_6)_2 \cdot H_2O$[b]	+1.12, −0.46[d]	

[a] Experimental conditions: 0.1 M tetrabutylammonium hexafluorophosphate ([TBA]PF_6), Pt-button working electrode, 20 °C, [complex] ~ 10^{-3} M. The redox potentials were measured against the internal standard ferrocenium/ferrocene, for which a redox potential in CH_3CN of +0.40 V vs NHE was assumed; the potentials are referenced vs the NHE. [b] CH_3CN solution. [c] Acetone solution. [d] Reversible. [e] Irreversible.

$[L_2Ru_2^{IV}(\mu\text{-}O)_3](PF_6)_2 \cdot H_2O$ do not rule out a metal–metal bond but do not provide conclusive evidence for it either.

Electrochemistry. (a) Monomeric Complexes. Cyclic voltammograms (CV) for monomeric $LRuX_3$ (X = Cl, Br, I) have been recorded in acetonitrile solutions (0.1 M [TBA]PF_6 supporting electrolyte) at a Pt-button working electrode at ambient temperature and scan rates of 20–200 mV/s. The results are summarized in Table VIII. The chloro and bromo complexes show a reversible one-electron oxidation wave at quite positive potentials, which corresponds to the couple $[LRuX_3]^{+/0}$. At negative potentials an irreversible reduction peak is observed for both complexes, which is assigned to the generation of $[LRu^{II}X_3]^-$ species that probably undergo halide substitution reactions with the solvent. At scan rates of >150 mV/s this process

$$[LRu^{IV}X_3]^+ \underset{+e^-}{\overset{-e^-}{\rightleftharpoons}} LRu^{III}X_3 \xrightarrow{+e^-} [LRu^{II}X_3]^- \rightarrow \text{dissociation products} \quad (2)$$

is quasireversible. Interestingly, the electrochemical oxidation of the monochloro and dichloroammineruthenium(III) complexes $[(NH_3)_5RuCl]^{2+}$ and $[Ru(NH_3)_4Cl_2]^+$ has not been observed, but their reversible reduction to ruthenium(II)[47] is a feasible process.

The CV for $[LRu(NCCH_3)_3](PF_6)_2$ in CH_3CN solution at a Au working electrode shows a reversible one-electron wave at +1.31 V vs NHE (eq 3). A coulometric measurement at +1.8 V confirmed a one-electron transfer (n = 0.94 ± 0.1).

$$[LRu(NCCH_3)_3]^{3+} + e^- \rightleftharpoons [LRu(NCCH_3)_3]^{2+} \quad (3)$$

It is noted that oxidation of $[Ru(NCCH_3)_6]^{2+}$ has not been observed up to +2.5 V.[26] This is a demonstration of the stabilization of the Ru^{II} oxidation state by six π-acceptor acetonitrile ligands, which is reduced by substitution of three of these one 1,4,7-trimethyl-1,4,7-triazacyclononane, which is a pure σ-donor. Clark and Ford[48] have estimated that one CH_3CN ligand stabilizes the II oxidation state of ruthenium by ≈0.4 V. This is nicely verified here. The redox potential of the couple $[Ru([9]aneN_3)_2]^{3+/2+}$ ([9]$aneN_3$ represents 1,4,7-triazacyclononane) is +0.37 V vs NHE.[45,49] From Ford's correlation, a redox potential of +1.5 V is calculated for $[LRu(NCCH_3)_3]^{3+/2+}$, which is to be compared with the experimental value of +1.3 V. The small difference of 0.2 V between the observed and calculated value may be due to a differing electronic effect of the two cyclic triamine donor ligands in both complexes (three secondary amine vs three tertiary amine N-donor atoms). The same correlation predicts a redox potential of ≈+2.7 V vs NHE for the $[Ru(NCCH_3)_6]^{3+/2+}$ couple.

(b) Binuclear Complexes. Figure 6 shows the CV of $[L_2Ru_2^{2.5}(\mu\text{-}Br)_3](PF_6)_2$ in acetone (0.1 M [TBA]PF_6) at a platinum working electrode in the potential range −0.5 V to +1.5 V vs Ag/AgCl reference electrode. Two reversible one-electron transfer processes are observed, which correspond to the couples designated in eq 4. The CV's of $[L_2Ru_2^{2.5}(\mu\text{-}Cl_3)](PF_6)_2$ in

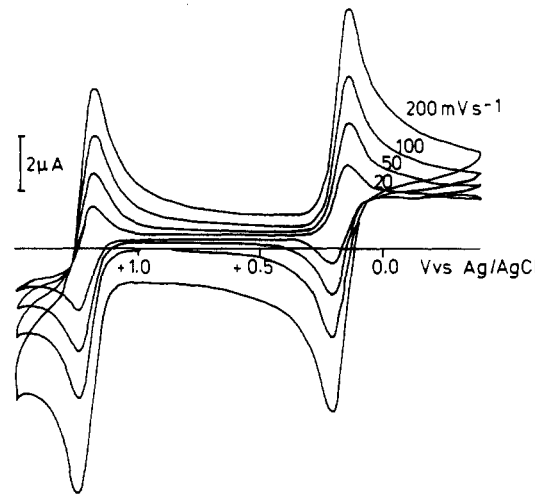

Figure 6. Cyclic voltammogram for $[L_2Ru_2(\mu\text{-}Br)_3](PF_6)_2$ in acetone (0.1 M [TBA] PF_6) at scan rates of 20, 50, 100 and 200 mV s^{-1} at a platinum-button electrode.

$$[L_2Ru_2^{III}X_3]^{3+} + e^- \underset{}{\overset{E^1_{1/2}}{\rightleftharpoons}} [L_2Ru^{II}Ru^{III}X_3]^{2+} + e^- \underset{}{\overset{E^2_{1/2}}{\rightleftharpoons}} [L_2Ru_2^{II}X_3]^+ \quad (4)$$

X = Cl, Br, I

acetonitrile and $[L_2Ru_2^{2.5}(\mu\text{-}I)_3](PF_6)_2$ in acetone solution are very similar. The redox potentials $E^1_{1/2}$ and $E^2_{1/2}$ are given in Table VIII.

The difference $|E^1_{1/2} - E^2_{1/2}|$ decreases on going from the μ-chloro- to the μ-bromo to the μ-iodo-bridged species. A measure of the stability of the mixed-valence complexes $[L_2Ru_2X_3]^{2+}$ is the comproportionation constant K_c as defined in eq 5. From

$$[L_2Ru_2^{III}X_3]^{3+} + [L_2Ru_2^{II}X_3]^+ \rightleftharpoons 2[L_2Ru_2^{2.5}X_3]^{2+} \quad K_c \quad (5)$$

the respective redox potentials, $E^1_{1/2}$ and $E^2_{1/2}$, values for K_c are calculated to be 4.4×10^{20} for X = Cl, 1.8×10^{17} for X = Br and 2.4×10^{14} for X = I. Thus the stability of the mixed-valence form decreases in the order μ-Cl > μ-Br > μ-I.

Similar redox behavior has been reported for a series of asymmetric complexes of the type $[(AsB_3)_{6-y}Cl_yRu_2(\mu\text{-}Cl_3)]^z$ (where B represents p-tolyl, p-chlorophenyl, and phenyl) and $[(PEt_2Ph)_{6-y}Cl_yRu_2(\mu\text{-}Cl_3)]^z$.[3a,b] Two reversible metal-centered one-electron-transfer processes were observed, and K_c varies from 2×10^9 to 2.6×10^{28}. The stability of the mixed-valence form increases with increasing asymmetry of the coordination spheres of the two Ru centers. Furthermore, substitution of the neutral ligands by halide ligands decreases the redox potential for the process $Ru_2^{III} + e^- \rightleftharpoons Ru^{II}Ru^{III}$, and consequently, $[Ru_2Cl_9]^{3-}$ may be oxidized to the $Ru^{III}Ru^{IV}$ species at electrochemically accessible potentials.[4]

The CV for $[L_2Ru_2^{2.5}(OH)_3](PF_6)_2 \cdot H_2O$ in acetonitrile at a platinum working electrode shows only one reversible one-electron-transfer process, $E_{1/2}$ = −0.11 V vs NHE. A second irreversible reduction peak is observed at −1.30 V. The former corresponds to the couple $[L_2Ru_2(OH)_3]^{3+/2+}$ whereas at a very negative potential an irreversible reduction to Ru_2^{II} occurs. Up to a potential of +2.2 V vs Ag/AgCl *no* further oxidation step has been detected. The $Ru^{III}Ru^{IV}$ oxidation level is not accessible under these conditions in complexes with three hydroxo bridges. A sample of $[L_2Ru_2^{III}(OH)_3](PF_6)_3$ displays an identical CV.

It is interesting that the replacement of three halide bridges in $[L_2Ru_2X_3]^{2+}$ complexes by three hydroxo groups shifts the redox potentials to more negative potentials by ≈1 V. This indicates that the mixed-valence $[L_2Ru_2^{2.5}(\mu\text{-}OH)_3]^{2+}$ complex is more readily oxidized to the $[l_2Ru_2^{III}(\mu\text{-}OH)_3]^{3+}$ form, which is a very stable species as compared to its $[L_2Ru_2^{III}(\mu\text{-}X)_3]^{3+}$ analogues.

(47) Elson, C. M.; Itzkovich, I. J.; Page, J. A. *Can. J. Chem.* **1970**, *48*, 1639.
(48) Clark, R. E.; Ford, P. C. *Inorg. Chem.* **1970**, *9*, 227.
(49) Bernhard, P.; Sargeson, A. M. *Inorg. Chem.* **1988**, *27*, 2582.

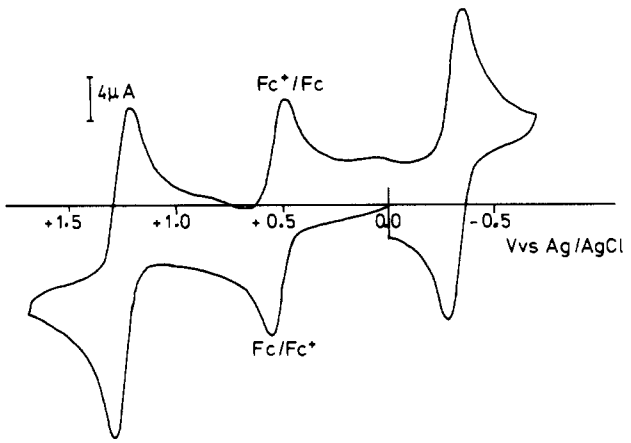

Figure 7. Cyclic voltammogram for $[L_2Ru_2(\mu\text{-}O)_3](PF_6)_2 \cdot H_2O$ in acetonitrile (0.1 M $[TBA]PF_6$) at a scan rate of 100 mV s^{-1} at a platinum-button electrode with ferrocene as internal standard.

This may be interpreted as evidence for the existence of comparatively stronger metal–metal bonding in the μ-hydroxo-bridged species. Upon oxidation of the mixed-valence form, an electron is removed from an antibonding molecular orbital of predominantly metal–metal character.

The CV for $[L_2Ru_2^{IV}(\mu\text{-}O)_3](PF_6)_2$ in acetonitrile is shown in Figure 7. In the potential range −0.7 to +1.7 V vs Ag/AgCl, two reversible one-electron waves are observed at $E^1_{1/2} = +1.12$ V and $E^2_{1/2} = -0.46$ V vs NHE. A coulometric measurement at 1.05 V vs Fc^+/Fc in nitromethane at a glassy-carbon working electrode established that the former corresponds to a one-electron oxidation of the binuclear Ru_2^{IV} species to the $Ru^{IV}Ru^V$ mixed-valence species ($n = 0.99 \pm 0.05$). The dark green color of the solution containing the Ru_2^{IV} complex changed to green-yellow during this oxidation, and the visible absorption spectrum of such an oxidized solution displays maxima at 416, 648, and 1320 nm. The CV recorded on such an oxidized solution was identical with the CV shown in Figure 7. This indicates that on the time scale of a coulometric measurement (≈30 min) the oxidized species is stable. The two one-electron-transfer reactions are thus assigned as in eq 6. Baar and Anson[50] have recently reported on the

$$Ru^{IV}Ru^V \underset{-e^-}{\overset{+e^-}{\rightleftharpoons}} Ru_2^{IV} \underset{-e^-}{\overset{+e^-}{\rightleftharpoons}} Ru^{III}Ru^{IV} \qquad (6)$$
$$E^1_{1/2} \qquad E^2_{1/2}$$

electrochemical behavior of dimeric complexes of $Ru^{III}Ru^{IV}$ and Ru_2^{IV} formed by oxidative dimerization of $[Ru^{III}(edta)OH_2]^-$. The probably oxo-bridged Ru_2^{IV} binuclear complex is capable of oxidizing water.

It is interesting that three μ-oxo bridging groups stabilize the Ru^{IV} oxidation state to such an extent that the $Ru^{IV}Ru^V$ level is readily accessible.

$[L_2Ru_2^{IV}(\mu\text{-}O)_3](PF_6)_2H_2O$ does not react with cyclohexane, ethanol, or benzyl alcohol. This may be due to the fact that the binuclear species is kinetically stable and has no labile coordination sites for substrate binding available.

Acknowledgment. We thank the Fonds der Chemischen Industrie for financial support of this work and the Degussa (Hanau, FRG) for a generous loan of $RuCl_3 \cdot xH_2O$. We are grateful to Professor P. Gütlich (Universität Mainz) for measuring the susceptibility of $[L_2Ru_2(\mu\text{-}O)_3](PF_6)_2 \cdot H_2O$ and Professor A. X. Trautwein (Medizinische Universität Lübeck) for measuring the ESR spectra.

Supplementary Material Available: A list of crystallographic details of the crystal structure determinations (Table S1) and tables of anisotropic displacement factors, H atom coordinates, bond lengths, and bond angles for **1** and **2** (9 pages); listings of observed and calculated structure factors for **1** and **2** (14 pages). Ordering information is given on any current masthead page.

(50) Baar, R. B.; Anson, F. C. *J. Electroanal. Chem. Interfacial Electrochem.* **1985**, *187*, 265.

Contribution from the Departments of Chemistry, Washington University, St. Louis, Missouri 63130, and Louisiana State University, Baton Rouge, Louisiana 70803-1804

Conformational Studies and Reduction Chemistry of a Bimetallic Cobalt(I) Carbonyl Complex Based on a Binucleating Hexakis(tertiary phosphine) Ligand System

Andre D'Avignon,[1a] Fredric R. Askham,[1a] and George G. Stanley*[,1b]

Received January 2, 1990

The 300- and 500-MHz ^1H NMR spectra of the bimetallic complex $Co_2(CO)_4(eHTP)^{2+}$ (eHTP = $(Et_2PCH_2CH_2)_2PCH_2P(CH_2CH_2PEt_2)_2$) show a number of solvent-dependent and, in the case of acetone, temperature-dependent shifts of the central methylene bridge and chelate ring proton resonances. The results of two-dimensional ^1H *J*-correlated experiments, with and without ^{31}P decoupling, are presented to assign both ^1H–^1H and ^1H–^{31}P coupling constants in acetone-d_6 and CD_2Cl_2. Broad-band ^{31}P decoupling causes a spectacular simplification of the highly coupled ^1H spectra, allowing clear resolution of all resonances. van der Waals energy calculations are presented for a model complex of $Co_2(CO)_4(eHTP)^{2+}$ that show the presence of several low-energy conformers differing by rotations about the central methylene bridge. The chemical shift changes for the P–CH_2–P proton resonances are proposed to be caused by differing amounts of carbonyl shielding from different rotational conformers in solution. The changes in the chelate ring proton resonances are proposed to be caused by trigonal-bipyramidal ⇄ square-pyramidal coordination geometry changes about the cobalt centers, which result in chelate ring conformational changes. The reduction of $Co_2(CO)_4(eHTP)^{2+}$ with naphthalenide anion produces the Co–Co-bonded dimer $Co_2(CO)_2(eHTP)$ in 40–50% yields. This very reactive material has been spectroscopically characterized, and both one-dimensional ^{31}P NMR and two-dimensional ^{31}P–^{31}P COSY NMR spectra for the product mixture are presented and discussed.

Introduction

The hexaphosphine ligand system $(Et_2PCH_2CH_2)_2PCH_2P(CH_2CH_2PEt_2)_2$, eHTP, was designed to both bridge and chelate two transition-metal centers, and we have found that this alkylated, electron-rich phosphine is an extremely powerful binucleating ligand system. So far every time we have added 2 equiv of a simple mononuclear metal halide (or related) complex we have obtained a bimetallic species, usually in high yield. Although the ligand was designed to produce closed-mode binuclear complexes such as **1a**, we have found that rotations about the central methylene group are facile and can produce open-mode complexes such as **1b** and **1c**, as well as a number of intermediate rotational conformations.

The first structurally characterized eHTP complex was $Co_2(CO)_4(eHTP)^{2+}$ (**2**), which was prepared from the reaction of 2

(1) (a) Washington University. (b) Louisiana State University.

0020-1669/90/1329-3363$02.50/0